

Scalable Creation of Deep Silicon-Vacancy Color Centers in Diamond by Ion Implantation through a 1- μm Pinhole

Lukas Hunold, Stefano Lagomarsino, Assegid M. Flatae, Haritha Kambalathmana, Florian Sledz, Silvio Sciortino, Nicla Gelli, Lorenzo Giuntini, and Mario Agio*

The controlled creation of quantum emitters in diamond represents a major research effort in the fabrication of single-photon devices. Here, the scalable production of silicon-vacancy (SiV) color centers in single-crystal diamond by ion implantation up to $\approx 1 \mu\text{m}$ depths is presented. The lateral position of the SiV is spatially controlled by a 1- μm pinhole placed in front of the sample, which can be moved nanometer precise using a piezo stage. The initial implantation position is controlled by monitoring the ion beam position with a camera. Hereby, silicon ions are implanted at the desired spots in an area comparable to the diffraction limit. The role of ions scattered by the pinhole and the activation yield of the SiV color centers for the creation of single quantum emitters is also discussed.

1. Introduction

Color centers in diamond are considered a very promising platform for quantum photonics devices due to their optical properties and the possibility to create diamond nanostructures.^[1–5]

L. Hunold, S. Lagomarsino, A. M. Flatae, H. Kambalathmana, F. Sledz, M. Agio

Laboratory of Nano-Optics and C μ
University of Siegen
Siegen 57072, Germany
E-mail: mario.agio@uni-siegen.de

S. Sciortino, N. Gelli, L. Giuntini
Istituto Nazionale di Fisica Nucleare
Sezione di Firenze
Sesto Fiorentino 50019, Italy

S. Sciortino, L. Giuntini
Department of Physics and Astronomy
University of Florence
Sesto Fiorentino 50019, Italy

M. Agio
National Institute of Optics
National Research Council (CNR)
Florence 50121, Italy

 The ORCID identification number(s) for the author(s) of this article can be found under <https://doi.org/10.1002/qute.202100079>

© 2021 The Authors. Advanced Quantum Technologies published by Wiley-VCH GmbH. This is an open access article under the terms of the Creative Commons Attribution-NonCommercial-NoDerivs License, which permits use and distribution in any medium, provided the original work is properly cited, the use is non-commercial and no modifications or adaptations are made.

DOI: 10.1002/qute.202100079

Among them, the negatively-charged silicon-vacancy (SiV) center has already achieved a number of important goals, such as bright emission concentrated in the zero-phonon line (ZPL),^[6] two-photon interference,^[7] spin preparation and readout,^[8] coherent dipole-dipole interaction,^[9] electroluminescence^[10] and single-photon emission in n-type diamond,^[11] temperature sensitivity^[12] and photostability even at high temperatures.^[13]

Color centers can be obtained either during diamond growth^[14] or by ion implantation followed by thermal annealing.^[15] Only in the second case their position can be laterally controlled, for instance by

focused ion-beam techniques^[16–18] or by aperture-type AFM tips,^[19] which is crucial for device fabrication. Although these techniques have demonstrated very high lateral resolution (down to about 10 nm), so far they have only been investigated at low ion energies (a few keV), which limits the implantation depth to only a few nanometers. It is therefore desirable to study the creation of color centers, in particular the SiV, in a broader range of ion energies to gain flexibility in terms of implantation depths. This can be used to avoid surface effects on the color centers and allows post-processing of the sample (e.g. surface etching, lithography), without destroying the emitters.

Here, we implement a commercial 1- μm pinhole and a high-precision translation stage into a beamline of a tandem accelerator to implant Si ions in spots comparable to the diffraction limit. This is done in a controlled manner, and in a wide range of energies (0.4–3 MeV) as well as fluences (10^8 – 10^{14} cm⁻²). In this way, we present a flexible and easy implementable approach for a localized implantation process down to single ions up to depths of about 1 μm . The pinhole size is chosen to 1- μm in order to compromise between ease of fabrication and low ion scattering on the one hand and precision on the other. Smaller pinholes can be used in the future, when being fabricated with vertical walls and low roughness. The fundamental precision limit is provided by ion straggling in diamond (about 100 nm for 3 MeV ion energy and 45 nm for 400 keV). We further investigate the role of ions scattered by the pinhole to determine the conditions for the creation of single SiV centers. Finally, we demonstrate the scalable generation of single emitters by measuring their antibunching characteristics.

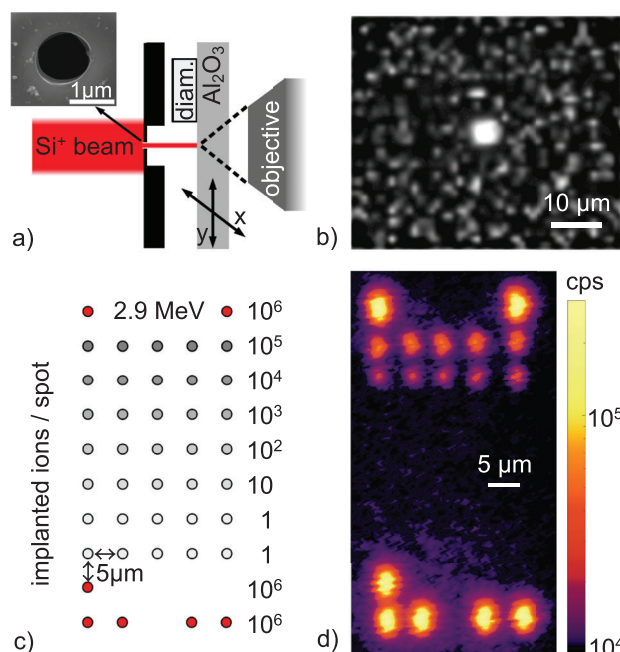


Figure 1. a) Implantation setup with pinhole, diamond sample on sapphire plate and objective sending the PL created by the beam to a camera. Sample and plate can be moved in x , y (perp. to the beam) with a piezo stage. Inset shows an SEM image of the $1\ \mu\text{m}$ pinhole. b) Beam image on the camera used to set the initial implantation position. c) Plan of implantation session A (compare Table 1 for session labeling). d) Corresponding PL map acquired by confocal scan.

2. Methods and Preparation

The implantation facility is described in detail in ref. [20]. In short terms, it consists of a 3 MV tandem accelerator employing a cesium sputter ion source able to form ion beams from solid state samples. The maximum energy depends on the ion state of charge, and amounts to 15 MeV in the case of silicon. Implantation takes place in a vacuum chamber downstream to the accelerator. The facility was previously used for versatile SiV color center creation^[21] and it has been upgraded with a system for localized implantation as described in the following. Annealing of the centers is carried out in an alumina oven surrounded by graphitic heaters, all placed in a stainless steel ultra-high vacuum chamber. The temperature is increased to 1150 °C within 2 h and kept there for one additional hour.

Figure 1a shows a scheme of the implantation setup. The beam enters the configuration from the left and passes the pinhole to reach a sapphire (Al_2O_3) plate. Here it produces a photoluminescence (PL) signal, which is monitored by a CMOS camera (ZWO ASI178MM) using a microscope objective. The PL spot is enlarged to about 5 pixels (see Figure 1b) in order to clearly discriminate it from hot pixels on the camera. The initial implantation position is then set by moving the sample into the beam until the desired location is reached. The absolute accuracy of this overall process is evaluated to approx. $\pm 5\ \mu\text{m}$ and it is limited by the resolution of the camera. The relative positioning of the following implantation spots is then very accurate and limited by the pre-

Table 1. Implantation sessions and corresponding parameters.

Implantation session	Energy [MeV]	Fluence [cm^{-2}]	Separation [μm]	Rows \times columns
A	2.9	10^8 – 10^{14}	5	10×5
B	0.4	10^8 – 10^{14}	5	10×5
C	1	10^9 – 10^{11}	10	3×8
D	0.4	10^{10}	10	1×5

cision of the translation stage (Q-545.240, Physik Instrumente GmbH, 26 mm travel range, 1 nm resolution).

The commercial pinhole is from Thorlabs (P1H) and it has a nominal diameter of $1\ \mu\text{m}$, with a tolerance of $+0.25/-0.1\ \mu\text{m}$ and a circularity of $\geq 80\%$. The scanning electron microscopy (SEM) picture (Figure 1a inset) indicates a smooth circular geometry and a diameter slightly larger than $1\ \mu\text{m}$, but within the specified tolerance. The foil thickness around it is measured optically to $d_{\text{foil}} = (27.5 \pm 1.1)\ \mu\text{m}$, which is important to evaluate a possible effect of a pinhole tilt on the ion throughput. We emphasize here, that for our $1\ \mu\text{m}$ hole, this issue is not as critical as in the case of nano-apertures.^[19] Nonetheless, the relatively thick frame of the pinhole demands a precise perpendicular mounting relative to the incoming ion beam. For the given system the horizontal and vertical tilt was measured to less than 0.3° , suitable for this implantation process.

Figure 1c illustrates a typical plan for an implantation matrix on an electronic grade diamond sample (ElementSix, $2 \times 2 \times 0.5\ \text{mm}^3$, face orientation 100, roughness 5 nm). The beam fluence is varied in order to generate spots with 10^6 to about 1 implanted ion with an energy of 2.9 MeV, corresponding to an implantation depth of around $1.1\ \mu\text{m}$. Matrices with other parameters have been created as well, the four most important ones for this work are summarized in Table 1.

After annealing, the PL signal of the formed emitters is acquired using a confocal scanning setup described in detail in ref. [22]. Figure 1d shows an exemplary result, reproducing the implanted matrix except for the spots with 10^3 Si ions or less. These are not visible, because their PL signal is overcome by a background noise associated with the diffuse implantation of ions scattered at the pinhole. This issue is discussed in Section 3 and it is studied in detail to eventually enable the identification of spots down to single emitters.

3. Results and Discussion

The implantation method introduced above, is used to create spots of color centers with a varying number of emitters for ion energies of 0.4 and 3 MeV. These are studied to extract information about the implantation process, the effect of ion scattering and the activation yield of SiV color centers at these energies. The experimental observations are compared to simulations of the process carried out with the SRIM tool.^[23] We then reduce the fluence successively down to the regime of single emitters and study a few of them as a proof of concept. The following sections describe these different steps further and present the

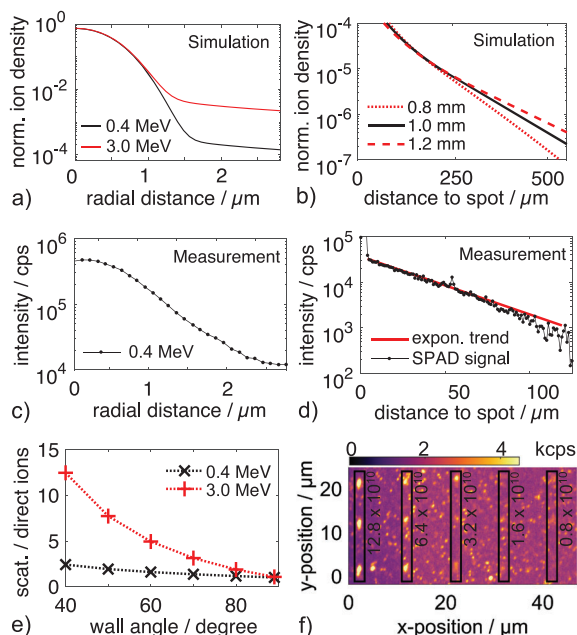


Figure 2. a) Simulated ion distribution around the desired spot on the sample, assuming 40° pinhole wall angle and a pinhole-sample distance of 1 mm. Two different ion energies are shown. b) Simulated far field ion distribution for the case of 3 MeV, 40° pinhole wall angle and three different pinhole-sample distances corresponding to the used value of (1 ± 0.2) mm. c) Example measurement for the ion distribution around the spot, showing the photon count rate of the SiV emission in this region. d) Example measurement of the long range SiV background for a strongly implanted spot. e) Ratio of total scattered to total direct ions for ion energies of 0.4 and 3 MeV as a function of the pinhole wall angle. f) Confocal scan of the matrix associated with C, showing scattered emitters around the desired spots. Fluences of the spots in the different columns are given in the figure (units cm^{-2}).

corresponding findings. More details on the used methods are to be found in Section 2.

3.1. Controlling Ion Scattering

Ions are scattered towards the sample by the pinhole, when its edges have thin parts allowing ions to be transmitted and distracted from their initial path by collisions within the material. We verify that this effect is relevant for our implantations by comparing the SiV signal around the created spots with simulations of the process carried out with the SRIM tool.^[23]

For this, we model the used pinhole with a conical shape and determine the amount of ions passing through its thin parts for a given energy. We then simulate the resulting trajectories after the pinhole and the corresponding distribution of ions on the sample for a given distance. We choose this distance to not more than 1 mm, resulting in an acceptable increase of the spot size due to beam divergence (measured to about 0.3 mrad). We further select an energy of 3 MeV for the simulations described above, resulting in the distance dependence of the implanted ion density as shown in **Figure 2a,b** for near and far regime, respectively. The experimental counterpart is obtained by measuring the SiV signal while moving away from the implanted spot (**Figure 2c,d**).

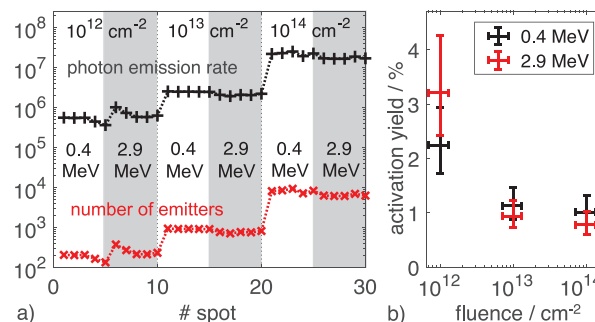


Figure 3. a) Photon emission rates (black curve) and corresponding emitter numbers (red curve) for highly implanted spots. Ten points were investigated for each fluence from 10^{12} cm^{-2} over 10^{13} cm^{-2} to 10^{14} cm^{-2} , as indicated by the values given in the figure. From those, always five were implanted with ion energies of 0.4 MeV (white columns) and five with 2.9 MeV (gray columns). b) Concluded activation yield of centers depending on energy and dose.

The spot size (FWHM) is in the range of 1–2 μm for different measured points, which is in agreement with the simulations that assume a beam divergence of 0.3 mrad and therefore a size of about 1.6 μm . A similar exponential decrease of the background resulting from scattered ions and thereby created SiV emitters is found, supporting the scattering model assumptions. It is also found that the measured background drops faster than expected, which might be attributed to uncertainties in the pinhole-sample distance or the simulations at the given energy and for the used pinhole material (steel).

The absolute strength of the shown background is determined by the number of scattered ions per directly implanted ion and it depends strongly on the ion energy and pinhole wall angle (**Figure 2c**). For 0.4 MeV, a value of 1–2 scattered ions per direct ion is calculated, depending on the pinhole wall angle. This result is acceptable, since the scattered ions are distributed over an area many orders of magnitude larger than the desired spot.

For the experiment, **Figure 2d** visualizes the predicted ion scattering, in the form of several bright spots around the implanted matrix points of implantation session C (see **Table 1**). Based on these results, the lower ion energy of 0.4 MeV is used for the creation of single emitters (session D, see **Table 1**) and stronger spots needed for initial localization of the matrix are placed further away ($>400 \mu\text{m}$ distance). With this, the scattered background is weak enough to create single emitters well separated from scattered ions.

3.2. Determination of the Activation Yield

The remaining task is to identify the appropriate beam fluence for the creation of a single emitter per spot (on average). For this the spots with a high number of emitters are studied first, which allow to quantify the activation yield of the color center conversion process. By using confocal intensity scans of the differently strong implanted spots, their SiV emission count rate is determined (**Figure 3a**, black curve). With the 2D intensity map it is possible to take into account that the laser only excites part of the spot when focused on it (by scaling up the signal with the ratio between spot and laser focus size).

Next, the number of emitters corresponding to these signals is calculated by using the average count rate of a single emitter as reference. This is estimated by averaging the signal of more than 300 bright spots found around the matrix of implantation session C (compare Figure 2d). By measuring the emission lifetime and spectrum of several random sample spots, it is verified that these are SiV color centers created by scattered ions. The relatively large separation (few micrometers) allows the assumption that most of them are single centers. In addition, spots with a size clearly larger than the diffraction limit are excluded. Therefore, the average signal of the remaining spots is seen as a good estimate for the single emitter count rate, which is evaluated to (2700 ± 300) cps under the given experimental conditions. Here, the used excitation laser power (3.3 mW at the sample surface), the excitation wavelength (656 nm), the NA of the focusing objective (0.95) and the overall collection and detection efficiency of the system (estimated to 0.12 %) are especially important. Higher single emitter count rates of previous studies can be attributed to the use of oil immersion objectives and more efficient detectors.^[17]

By maintaining these parameters for the measurements on the strongly implanted spots, the number of emitters per spot (Figure 3a, red curve) can be calculated. Based on this, the SiV activation yield is concluded for the given fluences (Figure 3b) (see Supporting Information for an estimation of the number of implanted ions, i.e., the pinhole throughput). Here the uncertainties are mainly due to instabilities in the beam current (error bars on the fluences) and to an imprecise determination of the pinhole throughput (error bars on the activation yield).

The values are in agreement with those reported in the literature^[15] for comparable energies, using a different and more direct method. They are also comparable to reported values for lower energies down to 100 keV,^[17] which indicates minor dependence of the activation yield on ion energies above the value of 100 keV. Accumulation of parasitic defects in the crystal lattice (e.g., vacancy clusters) is seen as one limiting factor for the formation of color centers. Although the number of created defects increases strongly for high ion energies, most of these are produced along the ion path and not at its final position. Therefore, this effect does not strongly depend on ion energy in agreement with the observed results. Another aspect is related to clustering of color centers, reducing the number of active emitters. This explains the reduced activation for increasing ion fluence, that is also observed in the measurements (compare Figure 3b).

3.3. Creation of Single Emitters

Next, the determined activation yield allows us to predict the number of created emitters also for spots with very low ion densities. If the activation remains constant for fluences below 10^{12} cm^{-2} , a value of $0.6 \times 10^{10} \text{ cm}^{-2}$ would provide roughly one activated emitter per spot on average. The assumption of constant activation yield at lower ion doses is supported by previous studies.^[17] To verify this, implantation session C is used. It consists of eight columns of emitter spots, starting with a fluence of $1.28 \times 10^{11} \text{ cm}^{-2}$ and reducing it by a factor of two for any of the following columns. Thereby transition between clear spots and single emitters is immediately evident (see Figure 2d). From the confocal scan, the column with 0.8×10^{10}

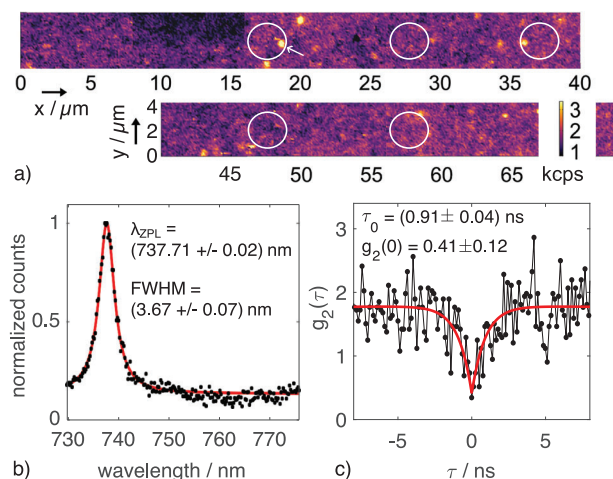


Figure 4. a) Confocal scan of the region around the matrix associated with session D. The expected positions of the matrix spots are indicated by the white circles. One of the identified emitters is marked with a white arrow. b) Emission spectrum of the marked spot. The Lorentzian fit shows a clear ZPL with the parameters given in the figure. c) Corresponding second order correlation measurement verifying the creation of a single SiV emitter by the presence of antibunching (deviation from zero due to background emission and electronic/photon noise). The used fit function corresponds to a three level model of the SiV center as derived in ref. [6].

cm^{-2} appears to be the first which reaches single emitters in the spots, supporting the results obtained by extrapolation from the strongly implanted spots.

Although some uncertainties are involved in the estimations above, the result allows the creation of spots with single emitters, because the number of activated centers per spot is assumed to follow a Poissonian distribution, as found also for example, in ref. [16]. Based on this, a mean number of 0.5–2 emitters per spot will statistically result in 25–35% spots with a single emitter. Therefore, single emitter creation is also possible under the above discussed conditions.

As proof of principle, five locations are implanted with a fluence of $1.6 \times 10^{10} \text{ cm}^{-2}$ in the context of session D. The confocal scan reveals almost no background associated with scattered ions (Figure 4a), in contrast to the previous approaches. Moreover, we further investigated the bright spots by measuring their spectral and temporal emission characteristics. Three of them are identified as SiV, out of which two are located within the expected regions (white circles). This indicates that the adjustments discussed above (lower ion energy, stronger spots at a larger distance) could create SiV centers at the desired locations, as shown by the Lorentzian fit exhibiting a clear ZPL (five/six times the sample background) around 738 nm (Figure 4b). Furthermore, the second order correlation measurements reveal antibunching behavior, verifying single-photon emission (Figure 4c). The used fit function in this case is

$$g_2(\tau) = 1 - [1 + a - g_2(0)] \cdot e^{-|\tau|/\tau_0} + a \cdot e^{-|\tau|/\tau_1} \quad (1)$$

according to the three-level model derived in ref. [6]. The extracted parameters are $a = 0.79 \pm 0.01$, $g_2(0) = 0.41 \pm 0.12$, $\tau_0 = (0.91 \pm 0.04) \text{ ns}$ and $\tau_1 = (425 \pm 8) \text{ ns}$, corresponding to the presence of a single emitter with pronounced shelving state.

Based on this, we conclude the general possibility of using the given concept for the localized creation of single color centers at higher depths.

4. Conclusion

In conclusion, we discuss the creation of SiV color centers by ion implantation through a 1- μm pinhole at desired locations in spots with size comparable to the diffraction limit. High energetic ions are used, which enables the formation of color centers deeper in the diamond, to allow post-processing of the sample and reduce surface effects on the emitters. A potential application is the post-fabrication of photonic structures around the formed color centers, in order to manipulate their photon emission characteristic.

We identify conditions for obtaining single emitters, including discussions of ion scattering by the pinhole and the activation yield. In particular, we describe the effect of ion energy on both of these aspects. We conclude no significant difference in color center activation for energies of 400 keV and 3 MeV, but reduced activation yield for increasing ion fluence, in agreement with literature on low energy implantations.^[17] Based on this, we demonstrate the ability to create SiV centers in a scalable manner, in a wide range of depths (energies).

We stress here that the possibility to create single emitters in a deterministic fashion is limited by the low activation yield of SiV color centers. This results in a Poisson distribution of active emitters per implanted spot, as observed in other experiments before,^[16] where only a fraction of spots exhibits single SiV color centers. This situation might be overcome by improving the activation yield or better by the development of deterministic activation techniques, like for the case of nitrogen vacancy centers.^[24]

The lateral precision can be improved by reducing the pinhole diameter down to the limit provided by ion straggling in diamond (about 100 nm for 3 MeV ion energy and 45 nm for 400 keV). In addition, a customized pinhole with vertical inner walls can be used to reduce ion scattering. It is also possible to change the pinhole to sample distance, if this is required for special applications. Moreover, the technique is general and can be applied to other ion species like, for example, nitrogen or germanium^[25] and other host matrices such as, for example, silicon carbide.^[26]

Supporting Information

Supporting Information is available from the Wiley Online Library or from the author.

Acknowledgements

The authors acknowledge financial support from the University of Siegen and the German Research Foundation (DFG) (INST 221/118-1 FUGG, 410405168). Experimental support was provided by N. Soltani (optical setup) and M. Hepp (SEM images) in association with the Micro- and Nanoanalytics Facility of the University of Siegen. The authors also acknowledge INFN-CHNet, the network of laboratories of the INFN for cultural heritage, for support and precious contributions in terms of instrumentation and personnel. The authors wish to thank F. Taccetti for experimental assistance and suggestions.

Open access funding enabled and organized by Projekt DEAL.

Conflict of Interest

The authors declare no conflict of interest.

Data Availability Statement

The data that support the findings of this study are available from the corresponding author upon reasonable request.

Keywords

diamond color centers, ion implantation, single-photon sources

Received: June 11, 2021
Revised: August 19, 2021
Published online: October 17, 2021

- [1] S. Pezzagna, D. Rogalla, D. Wildanger, J. Meijer, A. Zaitsev, *New J. Phys.* **2011**, *13*, 035024.
- [2] T. Schröder, S. L. Mouradian, J. Zheng, M. E. Trusheim, M. Walsh, E. H. Chen, L. Li, I. Bayn, D. Englund, *J. Opt. Soc. Am. B* **2016**, *33*, B65.
- [3] A. Sipahigil, R. E. Evans, D. D. Sukachev, M. J. Burek, J. Borregaard, M. K. Bhaskar, C. T. Nguyen, J. L. Pacheco, H. A. Atikian, C. Meuwly, R. M. Camacho, F. Jelezko, E. Bielejec, H. Park, M. Lončar, M. D. Lukin, *Science* **2016**, *354*, 847.
- [4] I. Aharonovich, E. Neu, *Adv. Opt. Mater.* **2018**, *2*, 911.
- [5] A. Sipahigil, M. D. Lukin, *Current Trends in Atomic Physics*, Oxford University Press, Oxford **2019**, pp. 1–28.
- [6] E. Neu, M. Agio, C. Becher, *Opt. Express* **2012**, *20*, 19956.
- [7] A. Sipahigil, K. Jahnke, L. Rogers, T. Teraji, J. Isoya, A. Zibrov, F. Jelezko, M. Lukin, *Phys. Rev. Lett.* **2014**, *113*, 113602.
- [8] L. J. Rogers, K. D. Jahnke, M. H. Metsch, A. Sipahigil, J. M. Binder, T. Teraji, H. Sumiya, J. Isoya, M. D. Lukin, P. Hemmer, F. Jelezko, *Phys. Rev. Lett.* **2014**, *113*, 263602.
- [9] R. E. Evans, M. K. Bhaskar, D. D. Sukachev, C. T. Nguyen, A. Sipahigil, M. J. Burek, B. Machielse, G. H. Zhang, A. S. Zibrov, E. Bielejec, H. Park, M. Lončar, M. D. Lukin, *Science* **2018**, *362*, 662.
- [10] A. Lohrmann, S. Pezzagna, I. Dobrinets, P. Spinicelli, V. Jacques, J.-F. Roch, J. Meijer, A. M. Zaitsev, *Appl. Phys. Lett.* **2011**, *99*, 25.
- [11] A. M. Flatae, S. Lagomarsino, F. Sledz, N. Soltani, S. S. Nicley, K. Haenen, R. Rechenberg, M. F. Becker, S. Sciortino, N. Gelli, L. Giuntini, F. Taccetti, M. Agio, *Diam. Relat. Mater.* **2020**, *105*, 107797.
- [12] C. T. Nguyen, R. E. Evans, A. Sipahigil, M. K. Bhaskar, D. D. Sukachev, V. N. Agafonov, V. A. Davydov, L. F. Kulikova, F. Jelezko, M. D. Lukin, *Appl. Phys. Lett.* **2018**, *112*, 203102.
- [13] S. Lagomarsino, F. Gorelli, M. Santoro, N. Fabbri, A. Hajeb, S. Sciortino, L. Palla, C. Czelusniak, M. Massi, F. Taccetti, L. Giuntini, N. Gelli, D. Y. Fedyanin, F. S. Cataliotti, C. Toninelli, M. Agio, *AIP Adv.* **2015**, *5*, 127117.
- [14] E. Neu, Ph.D. Thesis, Universität des Saarlandes **2012**.
- [15] S. Lagomarsino, A. M. Flatae, S. Sciortino, F. Gorelli, M. Santoro, F. Tantussi, F. De Angelis, N. Gelli, F. Taccetti, L. Giuntini, M. Agio, *Diam. Relat. Mater.* **2018**, *84*, 196.
- [16] S. Tamura, G. Koike, A. Komatsubara, T. Teraji, S. Onoda, L. P. McGuinness, L. Rogers, B. Naydenov, E. Wu, L. Yan, F. Jelezko, T. Ohshima, J. Isoya, T. Shinada, T. Tani, *Appl. Phys. Express* **2014**, *7*, 115201.
- [17] T. Schröder, M. E. Trusheim, M. Walsh, L. Li, J. Zheng, M. Schukraft, A. Sipahigil, R. E. Evans, D. D. Sukachev, C. T. Nguyen, J. L. Pacheco, R. M. Camacho, E. S. Bielejec, M. D. Lukin, D. Englund, *Nat. Commun.* **2017**, *8*, 15376.

- [18] Y. Zhou, Z. Mu, G. Adamo, S. Bauerdick, A. Rudzinski, I. Aharonovich, W.-b. Gao, *New J. Phys.* **2018**, *20*, 125004.
- [19] N. Raatz, C. Scheuner, S. Pezzagna, J. Meijer, *Phys. Status Solidi A* **2019**, *216*, 1900528.
- [20] S. Lagomarsino, S. Sciortino, N. Gelli, A. M. Flatae, F. Gorelli, M. Santoro, M. Chiari, C. Czelusniak, M. Massi, F. Taccetti, M. Agio, L. Giuntini, *Nucl. Instrum. Methods Phys. Res. B* **2018**, *422*, 31.
- [21] S. Lagomarsino, A. M. Flatae, H. Kambalathmana, F. Sledz, L. Hunold, N. Soltani, P. Reuschel, S. Sciortino, N. Gelli, M. Massi, C. Czelusniak, L. Giuntini, M. Agio, *Front. Phys.* **2021**, *8*, 601362.
- [22] H. Kambalathmana, A. Flatae, L. Hunold, F. Sledz, J. Müller, M. Hepp, P. Schmuki, M. Killian, S. Lagomarsino, N. Gelli, S. Sciortino, L. Giuntini, E. Wörner, C. Wild, B. Butz, M. Agio, *Carbon* **2021**, *174*, 295.
- [23] J. F. Ziegler, M. Ziegler, J. Biersack, *Nucl. Instrum. Methods Phys. Res. B* **2010**, *268*, 1818.
- [24] Y.-C. Chen, B. Griffiths, L. Weng, S. S. Nicley, S. N. Ishmael, Y. Lekhai, S. Johnson, C. J. Stephen, B. L. Green, G. W. Morley, M. E. Newton, M. J. Booth, P. S. Salter, J. M. Smith, *Optica* **2019**, *6*, 662.
- [25] T. Iwasaki, F. Ishibashi, Y. Miyamoto, Y. Doi, S. Kobayashi, T. Miyazaki, K. Tahara, K. D. Jahnke, L. J. Rogers, B. Naydenov, F. Jelezko, S. Yamasaki, S. Nagamachi, T. Inubushi, N. Mizuochi, M. Hatano, *Sci. Rep.* **2015**, *5*, 19587.
- [26] S. Castelletto, B. C. Johnson, V. Ivády, N. Stavrias, T. Umeda, A. Gali, T. Ohshima, *Nat. Mater.* **2014**, *13*, 151.